catalysts

MDPI

Article

Synthesis and Characterization of Supported Pd Catalysts for Potential Application in Glycerol Electro-Oxidation

Talent Ngwenya [1], Nolwazi Nombona [2] and Mzamo Shozi [1,*]

[1] School of Chemistry and Physics, University of KwaZulu-Natal, Durban 4000, South Africa; 211507267@stu.ukzn.ac.za
[2] Department of Chemistry, University of Pretoria, Pretoria 0001, South Africa; nolwazi.nombona@up.ac.za
* Correspondence: shozim2@ukzn.ac.za; Tel.: +27-312603105

Abstract: Ceria-supported Pd catalysts encompassing oxides of Cu, Co, and Fe were synthesized and characterized using XRD, TEM, SEM-EDX, TPR, BET, and Raman. After the incorporation of the metal oxides, the surface area and pore volume of the ceria support decreased. XRD showed the presence of the metal oxide phases as well as the support, CeO_2. TPR showed that the bimetallic catalyst had improved reducibility compared to the monometallic Pd/CeO_2. TEM images showed irregular-shaped particles with an average size distribution of 2–10 nm. SEM-EDX showed that the metal oxides were evenly distributed over the surface of the support. The electro-oxidation of glycerol in an alkaline environment was evaluated using cyclic voltammetry, and the products formed were identified and quantified using GC-MS. Glyceric acid was the dominant product over Pd-CuO/CeO_2, while glyceraldehyde and dihydroxyacetone were dominant over Pd-Co_3O_4/CeO_2 and Pd-Fe_2O_3/CeO_2, respectively.

Keywords: palladium; supported catalysts; glycerol; electro-oxidation; cyclic voltammetry

check for updates

Citation: Ngwenya, T.; Nombona, N.; Shozi, M. Synthesis and Characterization of Supported Pd Catalysts for Potential Application in Glycerol Electro-Oxidation. *Catalysts* **2022**, *12*, 192. https://doi.org/10.3390/catal12020192

Academic Editor: Ewa Kowalska

Received: 20 December 2021
Accepted: 17 January 2022
Published: 3 February 2022

Publisher's Note: MDPI stays neutral with regard to jurisdictional claims in published maps and institutional affiliations.

Copyright: © 2022 by the authors. Licensee MDPI, Basel, Switzerland. This article is an open access article distributed under the terms and conditions of the Creative Commons Attribution (CC BY) license (https://creativecommons.org/licenses/by/4.0/).

1. Introduction

Glycerol is used as a feedstock in the production of many valuable chemicals. It is the main by-product in the transesterification of vegetable oil into biodiesel. An increase in the glycerol supply has prompted the development of new applications for it in order to make the biodiesel industry more profitable [1,2]. The electro-oxidation of glycerol is an interesting reaction for its potential application in fuel cells and in electrochemical synthesis. Glycerol can be converted into a variety of fine chemicals (mono-alcohols, diols, ketones and carboxylic acids) via electro-oxidation [3,4].

The oxidation of glycerol forms a number of useful products such as dihydroxyacetone (DHA), which is used as an artificial tanning agent in cosmetics; tartronic acid (TA), which is an additive in candy, drinks, and wine; glyceric acid (GA), which is used in polymers and biodegradable emulsifiers; and mexosalic acid (MA), which is a biomarker in foods [1,5]. The commonly used metals for this oxidation reaction include Pt, Au, and Pd [6,7]. Au tends to be active at high potentials and thus is used as a promoter of transition metal oxides. Pd has been commonly used as an electrode material due to it high electrocatalytic activity in alkaline solution and its good poisoning tolerance in electro-oxidation reactions [8]. It has been shown that in alkaline media, Pd outperforms Pt and Au with higher current outputs. Simões et al. [9] used Pd/C, Au/C, $Pd_{0.5}Ni_{0.5}$/C, and $Pd_{0.5}Au_{0.5}$/C to evaluate glycerol electro-oxidation in alkaline media to produce value-added chemicals and energy cogeneration. They reported that bimetallic PdAu presents a shift of the onset potential almost 0.1 V toward lower potentials than the monometallic Au/C and Pd/C catalysts. Furthermore, at potentials between 0.7 and 0.9 V vs. RHE (reversible hydrogen electrode), Pd is found to be the most electro-active.

Kwon et al. [10] studied the mechanism of glycerol oxidation over Au under alkaline media using chromatography and electrochemical mass spectrometry techniques. On the Pt electrode, they reported that glyceric acid was formed via a glyceraldehyde pathway, while on the Au electrode, glyceric acid was reported to further oxidize to glycolic acid and formic acid at high potential. Glyceric acid, observed as the first product, showed that glyceraldehyde must be an intermediate oxidation product. In addition, they dismissed the possibility of CO_2 and HCOO-formation. Bianchini and Shen [11] reported that Pd/C promoted with metal oxides has superior activity for glycerol oxidation in alkaline media over Pt/C with 63% conversion and 58.5% selectivity to glyceraldehyde. In addition to the alloying approach, modifying Pd with oxides has been reported to be superior to Pd/C catalysts for alcohol oxidation [12].

In this study, we report the synthesis and characterization of ceria-supported Cu, Fe, and Co metal oxides promoted with Pd for potential application in the electro-oxidation of glycerol in alkaline media. These metal oxides were chosen with the focus on cost-effective transition metal-based catalysts. Furthermore, metal oxide nanoparticles have been reported to enhance the electrocatalytic performance of Pd due to their rich redox chemistry [13]. The catalysts prepared in this work offer a cheaper and economically viable alternative to traditional platinum group metals catalysts. Ceria was used as support due to its oxygen vacancies, which facilitates mass transfer whilst stabilizing the palladium species. Ceria produces oxygenated species during alcohol oxidation, thus facilitating the process [14].

2. Results and Discussion

2.1. Catalyst Characterization

2.1.1. Physicochemical Characterization

The textural properties of the synthesized catalysts are shown in Table 1. The metal loadings on the support were determined by ICP and were close to the desired loadings. When the metal oxides were loaded onto the ceria support, the surface area and pore volume of the support decreased as the metal oxide particles partially blocked the surface as well as the pores of the support, making the pores less accessible to N_2 molecules during BET analysis. Figure S1 in the Supplementary Materials shows the BET isotherms of the catalysts, which are type IV and H3 hysteresis loops [15]. H3 hysteresis loops indicate that the particles are mesoporous and their diameters range from 2 to 50 nm [16]. This is evident in the pore size distribution curves of the catalysts in Figure S2 in the Supplementary Materials.

Table 1. Physicochemical properties of the prepared materials.

	Metal Oxide Loading [a] (wt%)	Pd Loading [b] (wt%)	Surface Area (m^2/g)	Pore Volume (cm^3/g)
CeO_2	-	-	17	0.11
Pd/CeO_2	-	0.50	6.5	0.07
$Pd\text{-}CuO/CeO_2$	15.0	0.39	2.6	0.0073
$Pd\text{-}Co_3O_4/CeO_2$	14.3	0.41	5.4	0.011
$Pd\text{-}Fe_2O_3/CeO_2$	14.1	0.44	3.1	0.019

[a] Nominal loading = 15 wt%; [b] Nominal loading = 0.5 wt%.

2.1.2. X-ray Diffraction

The X-ray diffractograms of the catalysts are shown in Figure 1. Ceria exhibited peaks at 2-theta values of ≈28, 33, 48, 57, 60, 70, 76, 80, and 89 corresponding to the fluorite structure (JCPDS No. 34-0394) [17]. The peaks for the copper catalyst at 2-theta values of ≈36, 38, 48, and 70 correspond to the monoclinic phase of CuO (JCPDS No. 48-1548) [18]. For the cobalt catalyst, peaks at 2-theta values of ≈33, 37, and 59 were assigned to spinel phase of Co_3O_4 (JCPDS No. 042-1467) [19]. For the iron catalyst, peaks at 2-theta values of ≈33, 48, 57, and 70 assigned to the hematite phase were observed (JCPDS No. 33-0664) [20].

Typical PdO peaks are expected to appear at around 35°, 43°, 55°, and 72° [21]. However, they were not observed due to the low palladium loading, which was below the detection limit of the diffractometer.

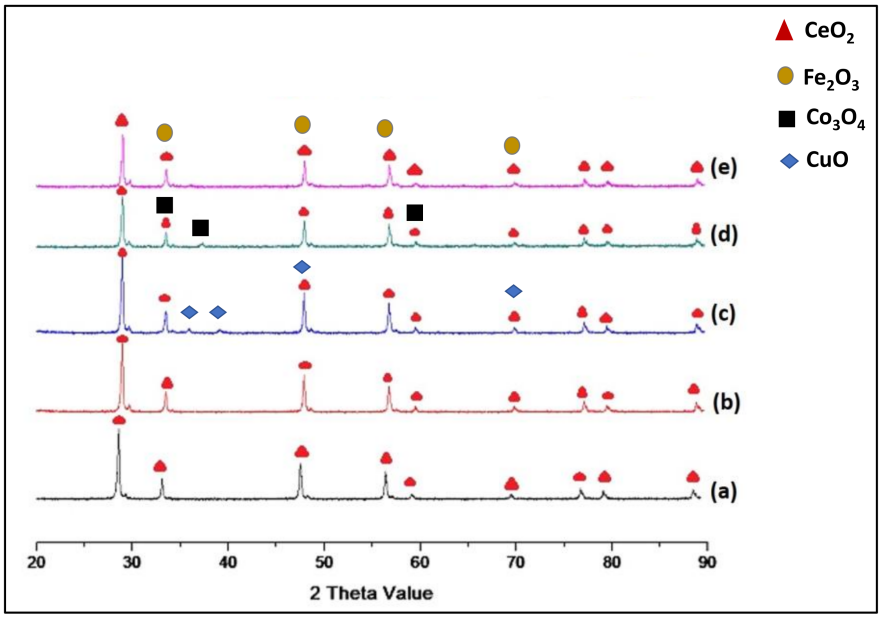

Figure 1. X-ray powder diffraction patterns of (**a**) CeO_2, (**b**) Pd/CeO_2, (**c**) $Pd\text{-}CuO/CeO_2$, (**d**) $Pd\text{-}Co_3O_4/CeO_2$, and (**e**) $Pd\text{-}Fe_2O_3/CeO_2$.

2.1.3. Temperature-Programmed Reduction

The H_2-TPR profiles of the catalysts are shown in Figure S3 in the Supplementary Materials, and their reduction temperatures and reducibility are shown in Table S1 in the Supplementary Materials. The profile of PdO/CeO_2 shows a reduction peak at 212 °C, which is assigned to the reduction of PdO to Pd where the metal loading is low [22]. For the Cu catalyst, only one reduction peak at 220 °C was observed, and this is attributed to the reduction of well-dispersed CuO to Cu [23]. $Pd\text{-}Co_3O_4/CeO_2$ showed two reduction peaks: at 131 °C attributed the reduction of Co^{3+} to Co^{2+} and at 256 °C attributed to the reduction of Co^{2+} to Co [24]. The peak at 131 °C could also be associated with the reduction of PdO as well as Co^{3+} to Co^{2+}. The presence of Pd(0) after this reduction favors H_2 spillover, which in turn causes an increase in the reducibility of the rest of the cobalt oxide species, allowing them to reduce at lower temperatures [25]. $Pd\text{-}Fe_2O_3/CeO_2$ also showed two peaks at 221 and 553 °C, which are attributed to the reduction of Fe^{3+} to Fe^{2+} and reduction of Fe^{2+} to Fe, respectively [26]. The degree of reducibility of the catalysts showed that the catalysts were not fully reduced; however, the reducibility was seen to improve from the Pd/CeO_2 when the Co, Cu, and Fe oxides were incorporated.

2.1.4. Electron Microscopy

The SEM-EDX images of the catalysts are shown in Figure 2. All catalyst exhibited a rocky surface morphology with irregularly shaped particles. The images show that for all catalysts, palladium is evenly dispersed on the surface with some areas rich in metal oxide. The bright-field TEM images and particle size distribution of the catalysts are shown in Figure S4 in the Supplementary Materials. The catalysts showed similar morphology and irregularly shaped particles with an average particle size distribution of 2–10 nm.

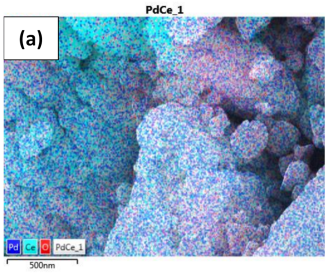

PdCe_1	wt%
O	15.81
Pd	0.44
Ce	83.75
Total	100.00

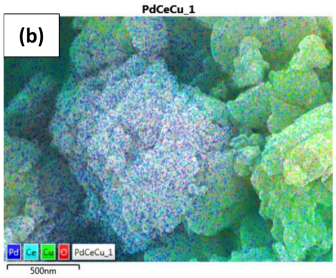

PdCeCu_1	wt%
O	19.89
Cu	30.07
Pd	1.70
Ce	48.34
Total	100.00

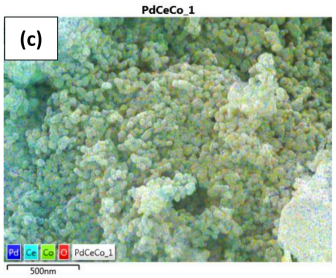

PdCeCo_1	wt%
O	25.64
Co	42.09
Pd	0.44
Ce	31.84
Total	100.00

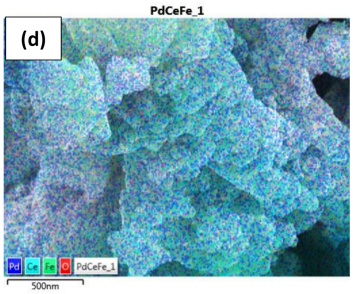

PdCeFe_1	wt%
O	21.42
Fe	12.16
Pd	0.76
Ce	65.65
Total	100.00

Figure 2. SEM-EDX images and corresponding wt% of each element of (**a**) Pd/CeO_2, (**b**) Pd-CuO/CeO_2, (**c**) Pd-Co_3O_4/CeO_2, and (**d**) Pd-Fe_2O_3/CeO_2 catalysts.

2.1.5. Raman Analysis

Figure 3 shows the Raman spectra of the synthesized catalysts. The Raman spectrum of Pd-CuO/CeO_2 showed three distinct bands. The band at 475 cm^{-1} is assigned to the F2g vibrational mode of the cubic fluorite structure of ceria in the catalyst. The bands appearing at 2335 cm^{-1} and 2912 cm^{-1} can be attributed to the presence of oxygen vacancies in the lattices of CeO_2 and CuO and the presence of CeO_2 defects [27]. Pd-Fe_2O_3/CeO_2 exhibited bands at 480 cm^{-1} and 810 cm^{-1} corresponding to vibrations of α-Fe_2O_3 [28]. For Pd-Co_3O_4/CeO_2, the prominent band at 475 cm^{-1} corresponds to the Eg mode of the Co_3O_4 crystalline phase [29], while the band at 805 cm^{-1} is assigned to A1g vibration mode of the crystalline Co_3O_4 phase [30].

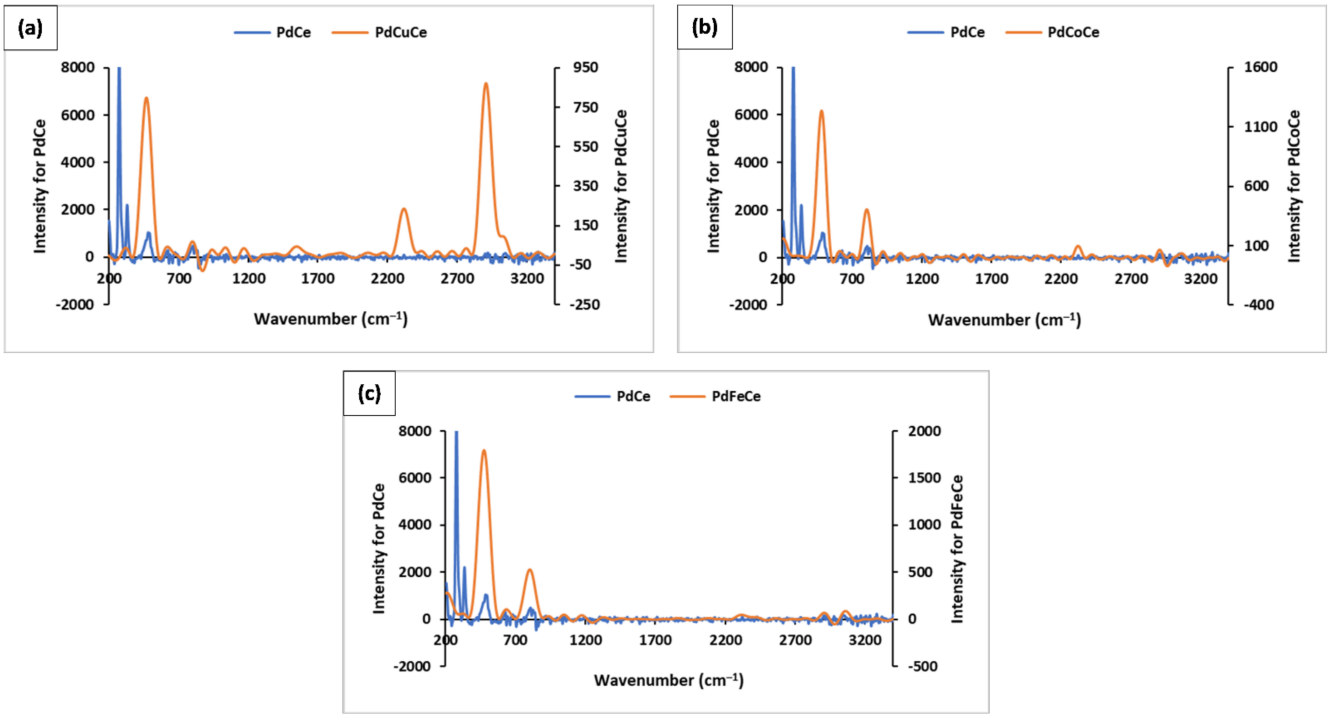

Figure 3. Raman spectra (orange) of (**a**) Pd-CuO/CeO_2, (**b**) Pd-Co_3O_4/CeO_2, and (**c**) Pd-Fe_2O_3/CeO_2 catalysts. The Raman spectrum of Pd/CeO_2 (blue) is included in all spectra for comparison.

2.2. Electrochemical Measurements

2.2.1. Electrochemical Properties of the Catalysts in Alkaline Media

The modified and unmodified electrodes were characterized using cyclic voltammetry (CV). Figure 4 shows the CV responses of the bare GCE and modified GCE in KOH solution. On the bare electrode, a weak irreversible peak was observed at ≈0.4 V. Upon modification with Pd/CeO2 (Figure 4ii), two processes (I and II) were observed. Process I at ≈0.2 V is reversible with an anodic to cathodic peak separation (ΔE) of 89 mV, and the current ratio is near unity. This process is assigned to the Ce^{3+}/Ce^{4+} redox process [31,32], as Ce is easily oxidized compared to Pd [33]. Process II at ≈0. 8 V is an irreversible process, which may be due to the oxidation of Pd [34]. Similar processes were observed for all catalysts. For the Pd-CuO/CeO_2 catalyst (Figure 4iii), a reversible process I was observed with redox peaks at E_{pa} = 0.30 V and E_{pc} = 0.11 V. The peak-to-peak-separation (ΔE) of this couple was determined to be 86 mV with a current ratio of 0.82. Redox peaks for the Pd-Co_3O_4/CeO_2 catalyst were observed at E_{pa} = 0.33 V and E_{pc} = 0.065 V with ΔE of 114 mV and a current ratio of 0.83. For the Pd-Fe_2O_3/CeO_2 catalyst's response (Figure 4v), process I showed a ΔE of 130 mV and current ratio of 0.77. The redox peaks were observed at E_{pa} = 0.29 V and E_{pc} = 0.11 V, and process II was observed at ≈0.8 V.

2.2.2. Electrochemical Behavior of the Catalysts in the Presence of Glycerol

The catalytic behavior of the catalysts was investigated in the oxidation of glycerol, and the CV responses are shown in Figure 5. Typically, the oxidation of glycerol occurs between 0.15 and 0.25 V on supported Pd catalysts [35]. The synthesized catalysts show redox peaks that overlap with the electrocatalytic glycerol oxidation peak.

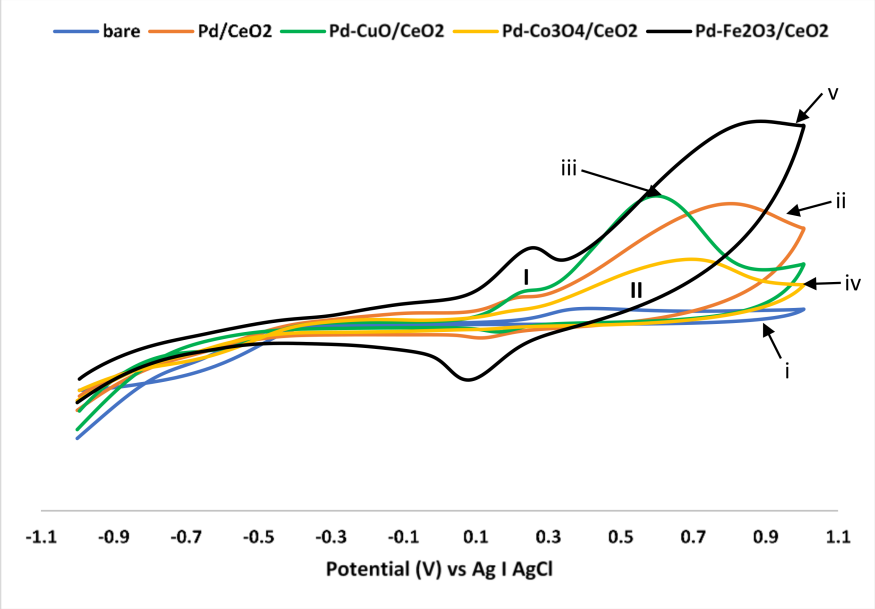

Figure 4. The CV response of GCE- (**i**) bare (**ii**) Pd/CeO_2, (**iii**) $Pd\text{-}CuO/CeO_2$, (**iv**) $Pd\text{-}Co_3O_4/CeO_2$, and (**v**) $Pd\text{-}Fe_2O_3/CeO_2$ catalysts in 1M KOH. Scan rate = 100 mV/s. Process I is the Ce^{3+}/Ce^{4+} redox process and Process II is an irreversible process due to the oxidation of Pd.

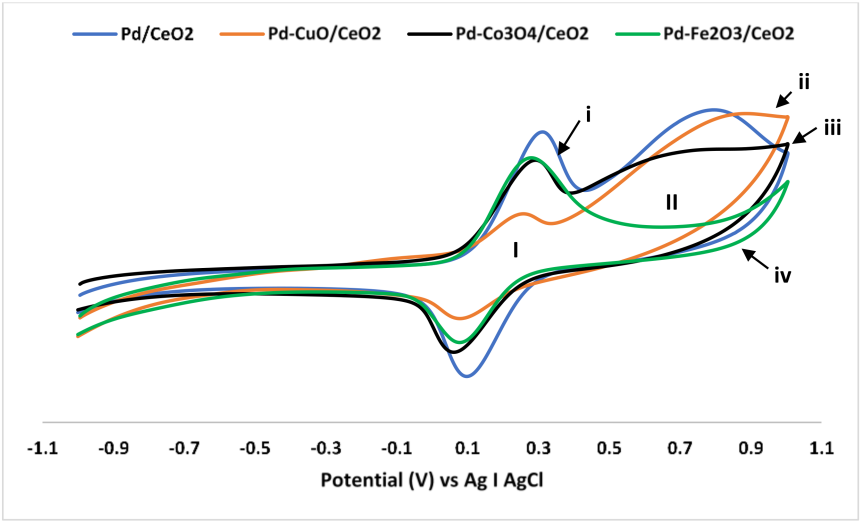

Figure 5. The CV response of GCE (**i**) Pd/CeO_2, (**ii**) $Pd\text{-}CuO/CeO_2$, (**iii**) $Pd\text{-}Co_3O_4/CeO_2$, and (**iv**) $Pd\text{-}Fe_2O_3/CeO_2$ in the presence of 1M KOH in 1M glycerol. Scan rate = 100 mV/s. Process I is the Ce^{3+}/Ce^{4+} redox process and Process II is an irreversible process due to the oxidation of Pd.

Measurement of the electroactive surface area (EASA) of these catalysts would allow one to study their activity and make comparisons with similar systems reported in the literature. However, this was not possible, as it has been reported that it is complex to evaluate the electroactive surface areas with the use of a bimetallic, as the estimation involves many uncertainties [36]. In order to confirm that the oxidation of glycerol took place, the solution was further analyzed using GC-MS. Table 2 shows the quantified products obtained. Glycerol oxidation can occur in two pathways [1]. In the first pathway, it is first converted to dihydroxyacetone, which is further converted to hydroxypyruvic acid and mesoxalic acid. The second pathway glycerol is oxidized to glyceraldehyde, which is further converted to glyceric acid. Glyceric acid was the dominant product over

Pd-CuO/CeO_2, while glyceraldehyde and dihydroxyacetone were dominant over Pd-Co_3O_4/CeO_2 and Pd-Fe_2O_3/CeO_2, respectively. Other products such as oxalic acid, formic acid, and glycolic acid were produced in low yields.

Table 2. Yield of glycerol oxidation products over the catalysts.

	Yield (%)			
	Pd/CeO_2	**Pd-CuO/CeO_2**	**Pd-Co_3O_4/CeO_2**	**Pd-Fe_2O_3/CeO_2**
glyceraldehyde	11	9	22	14
dihydroxyacetone	14	19	18	18
glyceric acid	26	21	12	10
mesoxalic acid	20	11	6	13
others *	10	6	4	5

* others: formic acid, glycolic acid, oxalic acid.

3. Materials and Methods

3.1. Catalyst Preparation

The catalysts were prepared via wet impregnation to obtain nominal loadings of 15 wt% of metal oxide (CuO or Fe_2O_3 or Co_3O_4) and 0.5 wt% Pd. Briefly, the supported metal oxides were prepared by impregnating the metal precursor [$Cu(NO_3)\cdot 3H_2O$ or $Fe(NO_3)_3\cdot 9H_2O$ or $Co(NO_3)_2\cdot 6H_2O$] onto ceria. After impregnation, the resulting material was dried overnight at 120 °C, which was followed by calcination at 550 °C in air. Then, the prepared supported metal oxides were doped with Pd by impregnating with an aqueous solution of $PdCl_2$ followed by drying overnight at 120 °C and calcination at 450 °C in air.

3.2. Catalyst Characterization

The surface area and porosity measurements were carried out using a Micromeritics Tristar II Surface area and Porosity Analyzer (Norcross, GA, USA). Samples were weighed and degassed overnight at 200 °C under a constant flow of nitrogen gas prior to analysis. Inductively coupled plasma analysis was performed using a Perkin Elmer Optical Emission Spectroscopy Optima 5300 DV (Waltham, MA, USA). Samples were digested in acid and then diluted accordingly prior to analysis. Powder X-ray diffraction was run using a Bruker D8 Advance (Karlsruhe, Germany) with Cu (Kα, λ = 1.5406 Å) as the radiation source. Raman spectroscopy was conducted using an Advantage 532 series spectrometer using Nuspec software (DeltaNu, WY, USA). The morphology of the catalysts was analyzed using Jeol JEM 1010 transmission electron microscopy (TEM) (Akishima, Japan) operated at an accelerating voltage of 100 kV. A small amount of sample was dispersed in ethanol and sonicated for 10 min prior to analysis and then loaded onto a copper grid. Elemental dispersion was determined using a FEG 1450 scanning electron microscopy (SEM) (Akishima, Japan) at 20 kV. Energy-dispersive X-ray (EDX) was performed using a Jeol JSM 6100 SEM (Akishima, Japan) equipped with a Bruker EDX detector (Karlsruhe, Germany) and analyzed using Espirit 1.8 software. Each sample was gold coated before analysis. Temperature-programmed reduction (TPR) analysis was carried out using a Micromeritics Autochem 2920 chemisorption analyzer (Norcross, GA, USA). Prior to reduction, approximately 50 mg of the sample was placed in a U-shaped quartz tube. During analysis, a mixture of dry ice/isopropanol was utilized, trapping the water produced in the process. The amount of hydrogen consumed during reduction was measured using a TCD.

3.3. Electrode Preparation and Electrochemical Measurements

Electrochemical measurements were carried out at room temperature with a conventional three-electrode configuration using a Metrohm 797 potentiostat (Herisau, Switzerland). The working electrode was a modified glassy carbon electrode (GCE). A Pt wire and AgCl were used as a counter and as a reference electrode. All solutions were de-aerated by bubbling pure nitrogen prior to each electrochemical experiment. Prior to modification, the bare glassy carbon electrode (GCE) was cleaned by successive sonication in absolute

ethanol, acetone, and Milli-Q water for 10 min. Then, the GCE was polished with alumina slurry and thoroughly rinsed with Milli-Q water. The modified electrode was prepared by drop casting a uniform suspension of either Pd/CeO_2, Pd-CuO/CeO_2, Pd-Co_3O_4/CeO_2, or Pd-Fe_2O_3/CeO_2 (10 mg, 10 mL ethanol, 1 mL of 5 wt% Nafion®) and dried for 10 min. The electrochemical behavior of the catalysts was assessed using cyclic voltammetry in alkaline media.

Supplementary Materials: The following are available online: https://www.mdpi.com/article/10.3390/catal12020192/s1. Figure S1: BET isotherms of the prepared catalysts, Figure S2: Pore size distributions of the prepared catalysts, Figure S3: H2-TPR profiles of the supported catalysts, Table S1: Summary of TPR data of the Pd catalysts, Figure S4: TEM images and corresponding particle size distribution of the catalysts.

Author Contributions: Conceptualization, T.N., N.N. and M.S.; methodology, T.N., N.N. and M.S.; formal analysis, T.N.; investigation, T.N.; resources, N.N. and M.S.; data curation, T.N.; writing—original draft preparation, T.N.; writing—review and editing, N.N. and M.S.; supervision, N.N. and M.S.; project administration, N.N. and M.S.; funding acquisition, N.N. and M.S. All authors have read and agreed to the published version of the manuscript.

Funding: This research was funded by the South African National Research Foundation, grant number 107090.

Data Availability Statement: Data are contained within the article and the Supplementary Materials.

Acknowledgments: We thank the Microscopy and Microanalysis Unit at University of KwaZulu-Natal for TEM and SEM analysis.

Conflicts of Interest: The authors declare no conflict of interest.

References

1. Walgode, P.M.; Faria, R.P.V.; Rodrigues, A.E. A review of aerobic glycerol oxidation processes using heterogeneous catalysts: A sustainable pathway for the production of dihydroxyacetone. *Catal. Rev.* **2021**, *63*, 422–511. [CrossRef]
2. Ladero, M. New glycerol upgrading processes. *Catalysts* **2021**, *11*, 103. [CrossRef]
3. Li, T.; Harrington, D.A. An overview of glycerol electrooxidation mechanisms on Pt, Pd and Au. *ChemSusChem* **2021**, *14*, 1472–1495. [CrossRef] [PubMed]
4. Ahmad, M.S.; Ab Rahim, M.H.; Alqahtani, T.M.; Witoon, T.; Lim, J.-W.; Cheng, C.K. A review on advances in green treatment of glycerol waste with a focus on electro-oxidation pathway. *Chemosphere* **2021**, *276*, 130128. [CrossRef]
5. Fan, L.; Liu, B.; Liu, X.; Senthilkumar, N.; Wang, G.; Wen, Z. Recent progress in electrocatalytic glycerol oxidation. *Energy Technol.* **2021**, *9*, 2000804. [CrossRef]
6. Wang, F.F.; Shao, S.; Li, C.-L.; Xu, C.-L.; Yang, R.-Z.; Dong, W.-S. Selective oxidation of glycerol over Pt supported on mesoporous carbon nitride in base-free aqueous solution. *Chem. Eng. J.* **2015**, *264*, 336–343. [CrossRef]
7. Thia, L.; Xie, M.; Liu, Z.; Ge, X.; Lu, Y.; Fong, W.E.; Wang, X. Copper-modified gold nanoparticles as highly selective catalysts for glycerol electro-oxidation in alkaline solution. *ChemCatChem* **2016**, *8*, 3272–3278. [CrossRef]
8. Habibi, E.; Razmi, H. Glycerol electrooxidation on Pd, Pt and Au nanoparticles supported on carbon ceramic electrode in alkaline media. *Int. J. Hydrog. Energy* **2012**, *37*, 16800–16809. [CrossRef]
9. Simoes, M.; Baranton, S.; Coutanceau, C. Electro-oxidation of glycerol at Pd based nano-catalysts for an application in alkaline fuel cells for chemicals and energy cogeneration. *Appl. Catal. B Environ.* **2010**, *93*, 354–362. [CrossRef]
10. Kwon, Y.; Lai, S.C.S.; Rodriguez, P.; Koper, M.T.M. Electrocatalytic oxidation of alcohols on gold in alkaline media: Base or gold catalysis? *J. Am. Chem. Soc.* **2011**, *133*, 6914–6917. [CrossRef]
11. Bianchini, C.; Shen, P.K. Palladium for alcohol oxidation in half cells and direct alcohol fuel cells. *Chem. Rev.* **2009**, *109*, 4183–4206. [CrossRef] [PubMed]
12. Wen, C.; Wei, Y.; Tang, D.; Sa, B.; Zhang, T.; Chen, C. Improving the electrocatalytic properties of Pd-based catalyst for direct alcohol fuel cells: Effect of solid solution. *Sci. Rep.* **2017**, *7*, 4907. [CrossRef] [PubMed]
13. Hu, T.; Wang, Y.; Liu, Q.; Zhang, L.; Wang, H.; Tang, T.; Chen, W.; Zhao, M.; Jia, J. In-situ synthesis of palladium-base binary metal oxide nanoparticles with enhanced electrocatalytic activity for ethylene glycol and glycerol oxidation. *Int. J. Hydrog. Energy* **2017**, *42*, 25951–25959. [CrossRef]
14. Yu, H.; Davydova, E.S.; Ash, U.; Miller, H.A.; Bonville, L.; Dekel, D.R.; Maric, R. Palladium-ceria nanocatalyst for hydrogen oxidation in alkaline media: Optimization of the Pd–CeO_2 interface. *Nano Energy* **2019**, *57*, 820–826. [CrossRef]
15. Sing, K.S.W. Reporting physisorption data for gas/solid systems with special reference to the determination of surface area and porosity (Recommendations 1984). *Pure Appl. Chem.* **1985**, *57*, 603–619. [CrossRef]

16. Rouquerol, J.; Avnir, D.; Fairbridge, C.W.; Everett, D.H.; Haynes, J.M.; Pernicone, N.; Ramsay, J.D.F.; Sing, K.S.W.; Unger, K.K. Recommendations for the characterization of porous solids (Technical Report). *Pure Appl. Chem.* **1994**, *66*, 1739–1758. [CrossRef]
17. Li, L.; Song, L.; Chen, C.; Zhang, Y.; Zhan, Y.; Lin, X.; Zheng, Q.; Wang, H.; Ma, H.; Ding, L.; et al. Modified precipitation processes and optimized copper content of CuO-CeO_2 catalyst for water-gas shift reaction. *Int. J. Hydrog. Energy* **2014**, *39*, 19570–19582. [CrossRef]
18. Zheng, S.; Zhang, W.; Silwa, M.; Su, H. Comparitive study of CeO_2/CuO and CuO/CeO_2 catalysts on catalytic performance for prefereantial CO oxidation. *Int. J. Hydrog. Energy* **2013**, *38*, 3597–3605. [CrossRef]
19. Choya, A.; de Rivas, B.; González-Velasco, J.R.; Gutiérrez-Ortiz, J.I.; López-Fonseca, R. On the beneficial effect of MgO promoter on the performance of Co_3O_4/Al_2O_3 catalysts for combustion of dilute methane. *Appl. Catal. A Gen.* **2019**, *582*, 117099. [CrossRef]
20. Lykaki, M.; Stefa, S.; Carabineiro, S.A.C.; Pandis, P.K.; Stathopoulos, V.N.; Konsolakis, M. Facet-dependent reactivity of Fe_2O_3/CeO_2 nanocomposites: Effect of ceria morphology on CO oxidation. *Catalysts* **2019**, *9*, 371. [CrossRef]
21. Simplício, L.M.T.; Brandão, S.T.; Domingos, D.; Bozon-Verduraz, F.; Sales, E.A. Catalytic combustion of methane at high temperatures: Cerium effect on PdO/Al_2O_2 catalysts. *Appl. Catal. A Gen.* **2009**, *360*, 2–7. [CrossRef]
22. Zhu, H.; Qin, Z.; Shan, W.; Shen, W.; Wang, J. Pd/CeO_2–TiO_2 catalyst for CO oxidation at low temperature: A TPR study with H_2 and CO as reducing agents. *J. Catal.* **2004**, *225*, 267–277. [CrossRef]
23. Sagar, G.V.; Rao, P.V.R.; Srikanth, C.S.; Chary, K.V.R. Dispersion and reactivity of copper catalysts supported on $Al_2O_2-ZrO_2$. *J. Phys. Chem. B* **2006**, *110*, 13881–13888. [CrossRef] [PubMed]
24. Garces, L.J.; Hincapie, B.; Zerger, R.; Suib, S.L. The effect of temperature and support on the reduction of cobalt oxide: An in situ X-ray diffraction study. *J. Phys. Chem. C* **2015**, *119*, 5484–5490. [CrossRef]
25. Ocsachoque, M.A.; Leguizamón-Aparicio, M.S.; Casella, M.L.; Lick, I.D. Promoting effect of palladium on $ZnAl_2O_4$-supported catalysts based on cobalt or copper oxide on the activity for the total propene oxidation. *Materials* **2021**, *14*, 4814. [CrossRef] [PubMed]
26. Musolino, M.G.; Busacca, C.; Mauriello, F.; Pietropaolo, R. Aliphatic carbonyl reduction promoted by palladium catalysts under mild conditions. *Appl. Catal. A Gen.* **2010**, *379*, 77–86. [CrossRef]
27. Zhang, X.; Wang, H.; Jiang, X.; Sun, H.; Qu, Z. Study of synergistic effect between CuO and CeO_2 over CuO@CeO_2 core–shell nanocomposites for NH_3-SCO. *Catal. Sci. Technol.* **2019**, *9*, 2968–2981. [CrossRef]
28. Bao, H.; Chen, X.; Fang, J.; Jiang, Z.; Huang, W. Structure-activity relation of Fe_2O_3–CeO_2 composite catalysts in CO oxidation. *Catal. Lett.* **2008**, *125*, 160–167. [CrossRef]
29. Dar, M.A.; Nam, S.H.; Abdo, H.S.; Almajid, A.A.; Kim, D.W.; Qurashi, A.; Kim, W.B. Self-assembled Co_3O_4 nanoplatelets into micro-spheres via a simple solvothermal route: Structural and electrochemical properties. *J. Alloys Compd.* **2017**, *695*, 329–336. [CrossRef]
30. Alvarez, A.; Ivanova, S.; Centeno, M.A.; Odriozola, J.A. Sub-ambient CO oxidation over mesoporous Co_3O_4: Effect of morphology on its reduction behavior and catalytic performance. *Appl. Catal. A Gen.* **2012**, *431–432*, 9–17. [CrossRef]
31. Wei, Y.; Fang, B.; Arai, T.; Kumagai, M. Electrolytic oxidation of Ce(III) in nitric acid and sulfuric acid media using a flow type cell. *J. Appl. Electrochem.* **2005**, *35*, 561–566. [CrossRef]
32. Chen, T.S.; Yeh, K.J.; Huang, K.L. Anion effects on the electrochemical regeneration of Ce(IV) in nitric acid used for etching chromium. *J. Hazard. Mater.* **2008**, *152*, 922–928. [CrossRef] [PubMed]
33. Boronin, A.I.; Slavinskaya, E.M.; Danilova, I.G.; Gulyaev, R.V.; Amosov, Y.I.; Kuznetsov, P.A.; Polukhina, I.A.; Koscheev, S.V.; Zaikovskii, V.I.; Noskov, A.S. Investigation of palladium interaction with cerium oxide and its state in catalysts for low-temperature CO oxidation. *Catal. Today* **2009**, *144*, 201–211. [CrossRef]
34. Mavrokefalos, C.K.; Hasan, M.; Khunsin, W.; Schmidt, M.; Maier, S.A.; Rohan, J.F.; Compton, R.G.; Foord, J.S. Electrochemically modified boron-doped diamond electrode with Pd and Pd-Sn nanoparticles for ethanol electrooxidation. *Electrochim. Acta* **2017**, *243*, 310–319. [CrossRef]
35. Fashedemi, O.O.; Ozoemena, K.I. Comparative electrocatalytic oxidation of ethanol, ethylene glycol and glycerol in alkaline medium at Pd-decorated FeCo@Fe/C core-shell nanocatalysts. *Electrochim. Acta* **2014**, *128*, 279–286. [CrossRef]
36. Trasatti, S.; Petrii, O.A. Real surface area measurements in electrochemistry. *Pure Appl. Chem.* **1991**, *63*, 711–734. [CrossRef]